11th International Conference on Fracture Mechanics of Concrete and Concrete Structures
FraMCoS-11
J. M. Chandra Kishen, A. Ramaswamy, S. Ray and R. Vidyasagar (Eds)
https://doi.org/10.21012/FC11.092320

MULTI-SCALE MODELING OF THE ELASTIC PROPERTIES OF HYDRATED CEMENT PASTE WITH CONSIDERATION OF ADHESION BETWEEN PHASES. REACTIVE MOLECULAR DYNAMICS SIMULATIONS AND HOMOGENIZATION

SELA HOEUN[*†], FABRICE BERNARD[†], FRÉDÉRIC GRONDIN[*], SIHAM KAMALI-BERNARD[†] AND SYED Y. ALAM[*]

[*] Nantes Université, École Centrale Nantes, CNRS, GeM, UMR 6183, F_44000 Nantes, France
e-mail: sela.hoeun@ec-nantes.fr, frederic.grondin@ec-nantes.fr,
syed-yasir.alam@ec-nantes.fr

[†] University of Rennes, INSA Rennes, Laboratoire de Génie Civil et Génie Mécanique (LGCGM),
20 avenue des Buttes de Coësmes 35700 Rennes, France
e-mail: fabrice.bernard@insa-rennes.fr, siham.kamali-bernard@insa-rennes.fr

Key words: Hydrated cement paste, Elastic constants, Molecular dynamics, Homogenization

Abstract: Hydrated cement paste is composed of three main phases (i.e., calcium-silicate-hydrates, portlandite, ettringite) and other hydrated phases. The aim of this study was to investigate the use of reactive molecular dynamics simulations to determine elastic constants of main hydrated cement paste composites taking into account adhesion between phases and using the open source code LAMMPS. Then, homogenization scheme was used to determine Young's modulus and Poisson's ratio of simplified hardened cement paste (HCP). Three composites of main hydrated cement paste phases were constructed to calculate the elastic constants, Young's modulus and Poisson's ratio. These composites are calcium-silicate-hydrates/calcium-silicate-hydrates, calcium-silicate-hydrates/portlandite and calcium-silicate-hydrates/ettringite. We have studied three configurations, which are 1 Å of vacuum layer, 3.1 and 6.2 Å of water layers between these composites, coupled with three different orientations. In order to obtain Young's modulus and Poisson's ratio of these composites, we used Voigt-Reuss-Hill (VRH) approximation scheme. After mechanical properties of composites were determined, we used Mori-Tanaka homogenization scheme to estimate Young's modulus and Poisson's ratio of simplified HCP. The calculation were shown to lead to the determination of Young's modulus in the range of 8.1 to 14. 6 GPa. This indicates that there is a possibility of obtaining Young's modulus of normal hardened cement paste from elastic constants calculations of different composites with other hydrated and unhydrated phases.

1 INTRODUCTION

Cement-based material is one of the most used materials in construction. It is generally characterized as a heterogeneous mixture. Concrete behaviour and in particular, its cracking remain relatively controlled because of this aspect. Mixture of cement matrix (a binding phase) and aggregates (a particulate phase) makes concrete. Hence, mechanical properties of concrete could be influenced by the cement matrix [1]. At different length scales, cement paste refers as a porous multiscale substance with varying physical properties [2]. At least 50% of total volume of hardened hydrated cement paste is calcium-silicate-hydrates (C-S-H) [3]. Portlandite (CH) is another major phase in hydrated Portland cement paste. The portlandite ignited mass

found by QXDA or thermal methods is generally in the range of 15-25% for typical Portland cements pastes cured for 3-12 months [4]. Ettrigite (AFt) is also an important phase to take into account especially in durability aspects. It is another hydration product of Portland, in particular super-sulphated and slag cements [5].

In order to model cement paste scale, mechanical properties of different phases of cement paste are required. One of method is to obtain those properties via nano-indentation experiments [6]. However, because of uncertainties from the smallest scale, it makes no negligible uncertainties at concrete scale. Therefore, it leads to the overestimation of structure and the use of security factors.

Advancement in the computational materials science and characterization of nanoscale structure of cementitious materials have made it possible for engineers and scientists to well understand and design concrete with a better durability and performance. Numerous numerical and/or analytical modeling works taking account of heterogeneity have been incrementally studied in civil engineering [6–8]. Nevertheless, the rupture of adhesion between hydrated cement phases is the cause of micro-cracking and damage of material rather than the rupture of the phases themselves (inter-phase and not intra-phase ruptures) [9].

In this paper, we present the method to acquire mechanical properties of the composite phases between the main cement paste phases using molecular dynamics (MD) simulations. This paper is organized as follows: (1) calculation of elastic constants, Young's modulus and Poisson's ratio through Voigt-Reuss-Hill (VRH) approximation of cement paste phases composites, and (2) calculation of Young's modulus and Poisson's ratio through Mori-Tanaka homogenization scheme of simplified hardened cement paste (HCP).

2 MATERIALS AND METHODS

2.1 Microstructure of hydrated cement

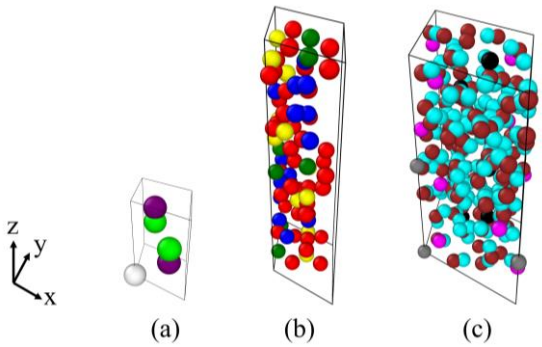

Figure 1: Calcium hydroxide, 11 Å tobermorite and ettringite unit cells in perspective view: (a) in CH phase, white balls is Ca atom, lime balls are H atoms, and purple balls are O atoms, (b) in 11 Å tobermorite phase, green balls are Ca atoms, yellow balls are Si atoms, red balls are O atoms, and blue balls are H atoms, and (c) in ettringite phase, gray balls are Al atoms, magenta balls are Ca atoms, cyan balls are H atoms, brown balls are O atoms, and black balls are S atoms.

In this study, portlandite (CH), ettringite (AFt) and calcium-silicate-hydrates (C-S-H) are considered. CH has cell lengths of a = b = 3.589 Å and c = 4.911 Å at room temperature and its chemical formula is $Ca(OH)_2$. CH unit cell was modelled following Desgranges et al. [10] as shown in **Fig. 1a**. Beside, AFt unit cell at 23 ^oC was modelled following Goetz-Neunhoeffer and Neubauer [11] with cell lengths of a = b = 11.229 Å and c = 21.478 Å as shown in **Fig. 1b**. AFt has chemical formula $Ca_6[Al_2(SO_4)_3(OH)_{12}]\cdot 26H_2O$. Both CH and AFt have trigonal space group ($P\bar{3}m1$) with cell angles (α, β, γ) = (90^0, 90^0, 120^0). For C-S-H phase, Fu [12] developed C-S-H (I) cell initially from 11 Å tobermorite. He did the annealing process to get C-S-H (I) with the Ca/Si ratio of 0.67. Our model was obtained following the same procedure. 11 Å natural tobermorite has a different space group unlike CH and AFt. It is a monoclinic crystal system P_21 with cell lengths of a = 6.69 Å, b = 7.39 Å and c = 22.779 Å as shown in **Fig. 1c** [13]. It has cell angle γ = 123.49^0 and chemical formula ($Ca_4Si_6O_{14}(OH)_4\cdot 2H_2O$).

2.2 Molecular dynamics and LAMMPS

Molecular dynamics is a computer simulation to calculate the equilibrium and transport characteristics of a classical many body system. The "classical" term means that the nuclear motion of constituent particles conforms to laws of classical mechanics. This could be a great approximation for numerous different types of materials [14].

Large-scale Atomic/Molecular Massively Parallel Simulator is known by the acronym LAMMPS. It is an open source code. Since the release in 2004, LAMMPS has a growth in popularity as a tool for particle-based modelling of materials at different length scales in a range of atomic to continuum scale [15].

2.3 Force field

Force field is quite vital for molecular dynamics simulations. In this study, Reactive Force Field (ReaxFF) [16] was chosen because it could be used with all the three phases (i.e., CH, C-S-H and AFt). Bonds between atoms are not necessarily created in the beginning of the simulation for using ReaxFF in LAMMPS. Therefore, it is suitable for modeling main cement paste phases composites, especially the interaction at the interface. Nevertheless, ReaxFF requires a lot of time to run each simulation. Its parameters could be obtained in Liu et al. [17].

Compared with empirical non-reactive force fields, ReaxFF divided energy of the system to different partial energy contributions as shown in **Eq. (1)** [16].

$$E_{system} = E_{bond} + E_{over} + E_{under} + E_{val} + E_{pen} + E_{tors} + E_{conj} + E_{vdW} + E_{Coul} \quad (1)$$

where E_{bond} is bond energy, E_{over} and E_{under} are energy penalty for over- and under-coordination of atoms, E_{val}, E_{pen}, E_{tors}, E_{conj}, E_{vdW} and E_{Coul} are valence angle, penalty, torsion, conjugation, Van der Waals and Coulombic energy, respectively.

2.4 Simulation procedure

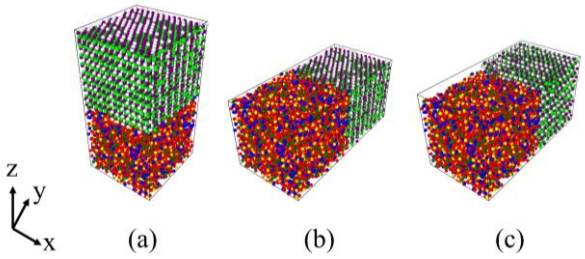

Figure 2: Orientations of C-S-H (I)/CH model: (a) CH supercell was put on top of C-S-H (I) supercell in z-direction, (b) CH supercell was put on the side of C-S-H (I) supercell in y-direction, and (c) counterclockwise rotated CH supercell around x-axis in yz plan was put on the side of CH supercell in y-direction.

In accordance with Hoeun et al. [18], these simulations were done in LAMMPS as 3D models with periodic boundary condition in x-, y- and z-directions. In order to get CH supercell, the replication of CH unit cell was firstly done 13, 16 and 9 times in x-, y- and z-directions, respectively. Similar to CH, C-S-H (I) and AFt were replicated to have C-S-H (I) and AFt supercells with the sizes of 7×8×2 and 4×5×2 in x-, y- and z-directions, respectively. These sizes of supercells were obtained for the sake of having similar lengths in all three dimensions. AFt was chosen as a reference because of its biggest size of unit cell among all three phases. In this way, it facilitated the replication of other phases. All colors of balls represents different types of atoms and they remain the same in this paper.

In an attempt to obtain independent results to each direction, individual supercells were changed from trigonal or monoclinic to orthogonal cells. Then energy minimization and relaxation with NPT ensemble for 50 ps at 0 atm and 300 K were applied on each supercell in x-, y- and z-directions. After placing supercells of different phases together, these composites were applied again under energy minimization and relaxation with the same procedure as individual supercells.

Three different orientations were chosen for composite simulations: (a) CH supercell on top of C-S-H (I) supercell in z-direction, (b) CH supercell on the side of C-S-H (I) supercell in y-direction and (c) counterclockwise rotated

CH supercell around x-axis in yz plane on the side of C-S-H (I) in y-direction as shown in **Fig. 2**. There were three different configurations: (a) 1 Å vacuum spacing, (b) 3.1 Å water spacing and (c) 6.2 Å water spacing were placed between C-S-H (I) and CH supercells as shown in **Fig. 3**.

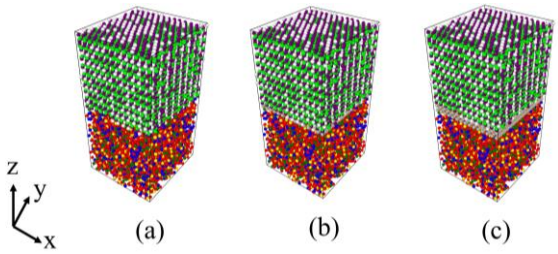

Figure 3: Configurations of C-S-H (I)/CH model: (a) C-S-H (I)/vacuum (1 Å)/CH, (b) C-S-H (I)/H_2O (3.1 Å)/CH, and (c) C-S-H (I)/H_2O (6.2 Å)/CH in z-direction. In water layer between supercells, silver balls are H atoms, and orange balls are O atoms.

In this study, deformations were applied on six different directions once at a time as could be seen in **Fig. 4**. Meanwhile, relaxation with NPT ensemble was maintained at 300 K and 0 atm in directions whose elastic constants were equal to zero. For instance, C_{51} and C_{61} were equal to zero in the trigonal space group. Thus NPT ensemble was relaxed in xz- and xy-directions. In order to obtain elastic constants, only a small deformation of 1% strain was required. For the purpose of sensitive analysis, different strain rates were tested by direct tension simulations. Hence, 10^{-6}/fs was the strain rate utilized in all simulations to get elastic constants.

Elastic constants were acquired from initial linear part of stress-strain curves obtained from simulations:

$$C_{ij} = \frac{\delta\sigma_i}{\delta\varepsilon_j} \qquad (2)$$

where $i,j = 1,2,3,4,5,6$, $\sigma_1 = \sigma_{xx}, \sigma_2 = \sigma_{yy}, \sigma_3 = \sigma_{zz}, \sigma_4 = \sigma_{yz}, \sigma_5 = \sigma_{xz}$ and $\sigma_6 = \sigma_{xy}$. Eventually, elastic constants were averaged along symmetric matrix.

Using Voigt-Reuss-Hill approximation, it was possible to acquire homogenized Young's modulus and Poisson's ratio. For different space groups, it should be noticed that calculations of shear and bulk moduli were also different.

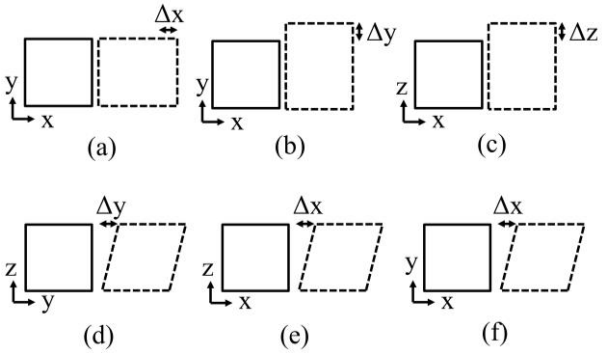

Figure 4: Six deformation directions: (a) tensile in x-direction, (b) tensile in y-direction, (c) tensile in z-direction, (d) shear in yz-plane, (e) shear in xz-plane, and (f) shear in xy-plane.

First, shear and bulk moduli of Voigt and Reuss bounds could be calculated. In the case of monoclinic space group (i.e., C-S-H (I)), details can be found in Wu et al. [19]. Then, arithmetic mean values were applied to the two moduli between Voigt and Reuss Bounds. With bulk and shear moduli, Young's modulus and Poisson's ratio might be acquired. There are seven mechanical stability conditions to be respected in the case of monoclinic space group [19]. The procedure is the same for trigonal space group, except that the expressions of shear and bulk moduli are different. Details can be found in Fu et al. [20]. In that case, there are three mechanical stability conditions to be respected for trigonal space group [20].

In this study, phase composition of hardened cement paste (HCP) with water-to-cement (w/c) ratio of 0.4 was used. We supposed that cement paste was well hydrated. Thus few unhydrated phases should be present. Then we considered a simplified hardened cement paste without taking into account unhydrated phases. Volume percentages of those phases are as follows: C-S-H phase represented by C-S-H (I) of 53%, CH phase of 19%, sulfoaluminate phase represented by AFt of 10% and capillary porosity of 18% [21]. Moreover, C-S-H gel includes low-density (LD) C-S-H about 70% and high-density (HD) C-S-H about 30% with gel porosity of 35% and 24%, respectively [22].

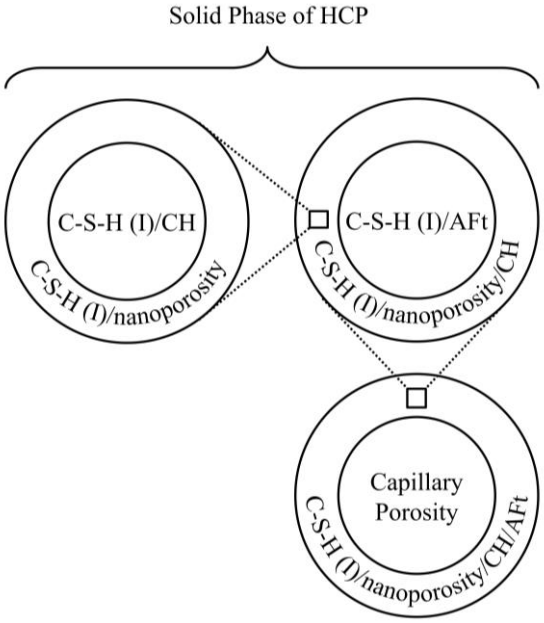

Figure 5: Homogenization scheme of simplified hardened cement paste.

In the study of Fu et al. [6], the assessment of the elastic modulus of LD and HD C-S-H through Mori-Tanaka and self-consistent schemes. They found that self-consistent scheme could be utilized to acquire Young's modulus no more than porosity volume fraction of 50%. And yet, Mori-Tanaka scheme could be utilized to acquire Young's modulus more than porosity volume fraction of 50%. In this study, Mori-Tanka scheme was chosen to calculate Young's modulus because the porosity volume fraction of the C-S-H (I)/nanoporosity is equal to 70%. Details of Mori-Tanaka homogenization procedure of simplified HCP are given in **Fig. 5**.

Firstly, Mori-Tanka homogenization scheme was applied on C-S-H (I) referred to matrix and nanoporosity referred to inclusion. Then C-S-H (I)/nanoporosity referred to matrix and C-S-H (I)/CH referred to inclusion were taken into account. Again, Mori-Tanaka scheme were applied on C-S-H (I)/nanoporosity/CH matrix referred to matrix and C-S-H (I)/AFt referred to inclusion. Finally, solid phase (i.e., matrix of C-S-H (I)/nanoporosity/CH/AFt) and capillary porosity referred to inclusion were taken into account in order to get a simplified HCP.

In order to calculate shear and bulk moduli of homogenous matrix, following equations of Mori-Tanka scheme could be used [32]:

$$K = \frac{\sum_r f_r k_r \left[1 + \alpha_s \left(\frac{k_r}{k_s} - 1\right)\right]^{-1}}{\sum_r f_r \left[1 + \alpha_s \left(\frac{k_r}{k_s} - 1\right)\right]^{-1}} \quad (3)$$

$$G = \frac{\sum_r f_r g_r \left[1 + \beta_s \left(\frac{g_r}{g_s} - 1\right)\right]^{-1}}{\sum_r f_r \left[1 + \beta_s \left(\frac{g_r}{g_s} - 1\right)\right]^{-1}} \quad (4)$$

where f_r is volume fraction of matrix, α_s and β_s coefficients are given by:

$$\alpha_s = \frac{3k_s}{3k_s + 4g_s} \quad (5)$$

$$\beta_s = \frac{6(k_s + 2g_s)}{5(3k_s + 4g_s)} \quad (6)$$

where g_r and g_s are shear moduli, k_r and k_s are bulk moduli of matrix and inclusion, respectively:

$$g_{r,s} = \frac{E_{r,s}}{2(1 + \mu_{r,s})} \quad (7)$$

$$k_{r,s} = \frac{E_{r,s}}{3(1 - 2\mu_{r,s})} \quad (8)$$

Shear and bulk moduli of water are 2.2 and 0 GPa, respectively. Poisson's ratio of water is equal to 0.5.

3 RESULTS AND DISCUSSION

In this study, reactive molecular dynamics simulations were chosen to acquire elastic constants of the main hydrated cement paste phases using LAMMPS. The results of elastic constants of different orientations, different configurations and different composites are summarize in **Tables 1-9**. By using obtained values of elastic constants, it is possible to calculate Young's modulus and Poisson's ratio via Voigt-Reuss-Hill (VRH) approximation as shown in **Figs. 6-8**. For C-S-H (I)/C-S-H (I) composite, Young's modulus and Poisson's ratio were respectively 48.8 GPa and 0.33 in the case of 1 Å vacuum spacing. When 3.1 and 6.2 Å water spacing were placed, Young's moduli dropped to the values of 41.2 and 21.8 GPa, respectively.

Table 1: Elastic constants (in GPa) of C-S-H (I)/C-S-H (I) in y-direction.

Spacing	1 Å vacuum	3.1 Å water	6.2 Å water
C_{11}	85.407	78.792	66.830
C_{22}	77.737	57.858	37.035
C_{33}	84.338	71.972	67.290
C_{44}	18.191	16.838	4.137
C_{55}	22.532	19.749	20.107
C_{66}	21.333	12.946	3.445
C_{12}	40.024	34.426	20.391
C_{13}	45.403	39.768	28.516
C_{15}	3.554	-1.084	-2.606
C_{23}	38.022	30.760	19.079
C_{25}	3.206	-1.871	-1.940
C_{35}	3.511	-0.182	0.454
C_{46}	1.502	-1.388	0.828

Table 2: Elastic constants (in GPa) of C-S-H (I)/C-S-H (I) in z-direction.

Spacing	1 Å vacuum	3.1 Å water	6.2 Å water
C_{11}	81.587	74.511	65.920
C_{22}	85.471	74.812	61.334
C_{33}	83.779	66.163	23.739
C_{44}	19.992	20.607	1.535
C_{55}	18.974	12.865	1.411
C_{66}	22.350	20.667	21.282
C_{12}	43.828	37.913	28.196
C_{13}	44.768	37.310	17.565
C_{15}	1.561	-0.491	0.668
C_{23}	46.012	36.321	15.158
C_{25}	2.137	-2.616	1.140
C_{35}	-1.187	-1.338	2.120
C_{46}	0.612	1.958	-0.991

To the knowledge of the authors, Liang [23] was the only one who investigate C-S-H/CH composite. They put CH phase on top of C-S-H phase composites with spacing about 3 Å. Young's modulus was obtained with value of about 40 GPa. In our study, Young's moduli of C-S-H (I)/CH composite obtained using VRH approximation with trigonal and monoclinic space groups were respectively 31.6 and 35.5 GPa in the case of 1 Å vacuum spacing. It seems that Young's modulus obtained by monoclinic space group is quite close to their results. It should be noticed that the methods to obtain Young's modulus are not the same. In their study, the values were obtained from stress-strain curves of uniaxial tensile test along z-direction. In our study, VRH approximation was utilized. It can be seen in **Figs. 6-8** that different orientations and configurations could lead to different results.

Table 3: Elastic constants (in GPa) of C-S-H (I)/C-S-H (I) counterclockwise rotated in y-direction.

Spacing	1 Å vacuum	3.1 Å water	6.2 Å water
C_{11}	68.320	63.005	56.045
C_{22}	64.077	53.620	35.109
C_{33}	38.005	33.177	31.801
C_{44}	11.606	10.071	4.439
C_{55}	13.340	9.548	11.597
C_{66}	17.729	15.424	2.739
C_{12}	28.686	24.910	17.651
C_{13}	21.490	15.780	13.429
C_{15}	1.837	1.474	-2.267
C_{23}	23.979	18.207	7.957
C_{25}	-0.337	1.874	-1.361
C_{35}	0.794	2.607	-0.762
C_{46}	0.634	-1.142	-0.721

For the first time, Young's modulus and Poisson's ratio of C-S-H (I)/AFt composite has been obtained. In the case of monoclinic space group, when interlayer spacing increased from 1 Å to 6.2 Å, Young's modulus of this composite dropped from 24.9 GPa to 13.6 GPa. Poisson's ratio otherwise increased from 0.36 to 0.39. At the same time, in the case of trigonal space group, Young's modulus dropped from 24.9 GPa to 15.2 GPa and Poisson's ratio increased from 0.37 to 0.39 which are quite close to results obtained for monoclinic space group. For the sake of comparison, no literature value could be found.

As can be seen in **Fig. 9**, Young's moduli and Poisson's ratios were averaged among three different orientations. Considering spacing between supercells similar to the one investigated by Bonnaud et al. [24] for C-S-H globules, Young's moduli of C-S-H (I)/C-S-H (I), C-S-H (I)/CH and C-S-H (I)/AFt are as follows: 41.2 GPa, 29.6 GPa and 21.9 GPa, respectively. For the last two values, they were obtained from mean values between trigonal and monoclinic space groups.

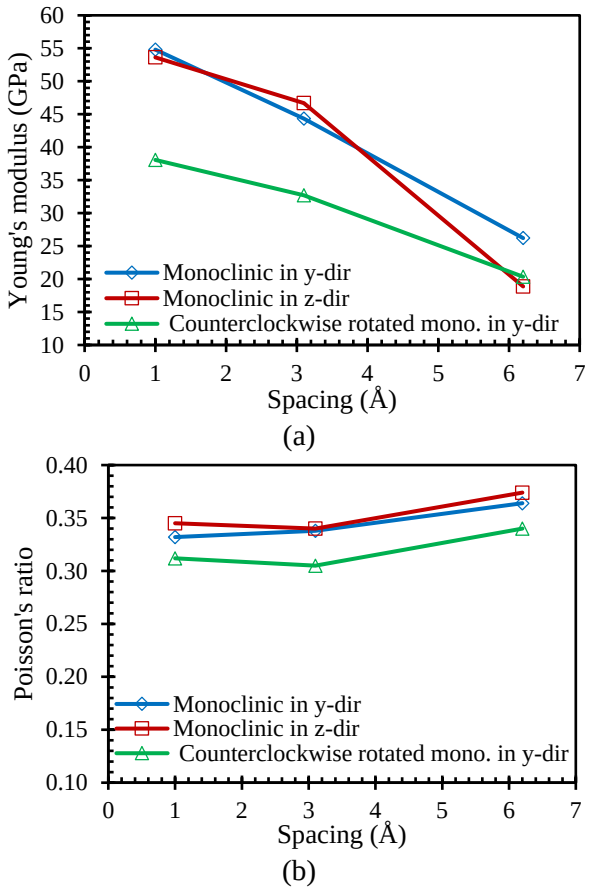

Figure 6: (a) Young's modulus, (b) Poisson's ratio in relation with spacing of C-S-H (I)/C-S-H (I) composites.

Table 4: Elastic constants (in GPa) of C-S-H (I)/CH in y-direction.

Spacing	1 Å vacuum	3.1 Å water	6.2 Å water
C_{11}	83.294	79.870	63.572
C_{22}	82.356	68.832	39.146
C_{33}	56.261	52.116	45.100
C_{44}	6.270	6.442	3.804
C_{55}	11.461	13.017	9.490
C_{66}	21.168	13.507	6.207
C_{12}	38.369	36.075	21.071
C_{13}	30.983	33.589	24.045
C_{15}	2.408	-0.724	-2.398
C_{23}	28.267	27.239	11.831
C_{25}	3.365	2.433	-0.744
C_{35}	1.154	3.081	-2.332
C_{46}	1.052	1.040	-3.733
C_{14}	-7.288	-5.343	-6.006
C_{24}	7.377	3.080	-2.456
C_{56}	-2.732	-0.139	-0.998

Table 5: Elastic constants (in GPa) of C-S-H (I)/CH in z-direction.

Spacing	1 Å vacuum	3.1 Å water	6.2 Å water
C_{11}	77.892	67.365	69.711
C_{22}	72.537	69.731	63.354
C_{33}	46.653	40.444	34.544
C_{44}	8.113	7.273	5.844
C_{55}	8.497	8.370	7.494
C_{66}	20.378	20.683	19.033
C_{12}	38.156	36.715	34.930
C_{13}	26.585	24.642	18.097
C_{15}	-0.233	0.053	1.260
C_{23}	22.474	21.285	15.392
C_{25}	-0.550	2.462	-0.146
C_{35}	-1.092	2.969	0.684
C_{46}	-1.258	0.741	-1.027
C_{14}	-6.156	-6.122	-2.257
C_{24}	4.340	7.019	3.130
C_{56}	-4.029	-4.238	-2.736

Table 6: Elastic constants (in GPa) of C-S-H (I)/CH counterclockwise rotated in y-direction.

Spacing	1 Å vacuum	3.1 Å water	6.2 Å water
C_{11}	67.389	67.216	63.722
C_{22}	39.742	35.521	32.780
C_{33}	36.321	33.475	32.303
C_{44}	6.241	4.301	6.679
C_{55}	15.955	10.484	13.264
C_{66}	11.828	10.847	5.907
C_{12}	19.946	17.688	18.240
C_{13}	18.609	19.213	17.792
C_{15}	-1.758	0.252	0.340
C_{23}	12.607	10.596	9.624
C_{25}	1.764	-0.054	1.246
C_{35}	-2.444	-0.454	0.485
C_{46}	-0.714	0.199	0.059
C_{14}	4.046	3.280	3.091
C_{24}	-2.391	-1.158	0.727
C_{56}	5.066	2.514	1.899

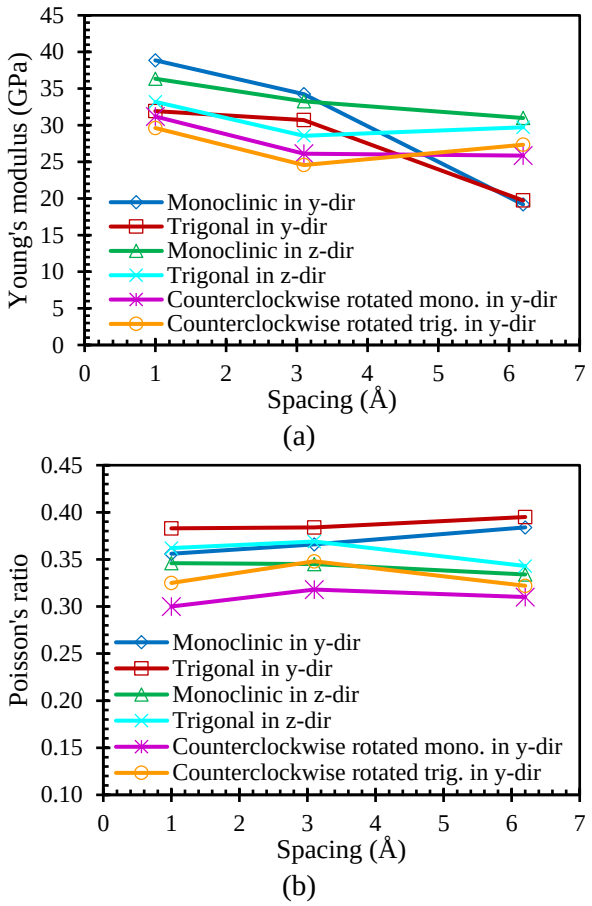

Figure 7: (a) Young's modulus, (b) Poisson's ratio in relation with spacing of C-S-H (I)/CH composite.

Table 7: Elastic constants (in GPa) of C-S-H (I)/AFt in y-direction.

Spacing	1 Å vacuum	3.1 Å water	6.2 Å water
C_{11}	49.995	46.941	40.820
C_{22}	28.906	31.023	23.964
C_{33}	58.024	57.747	55.068
C_{44}	4.038	4.012	2.452
C_{55}	9.844	11.543	9.171
C_{66}	6.448	2.168	2.281
C_{12}	19.561	15.933	14.140
C_{13}	22.879	22.731	21.596
C_{15}	1.5719	0.487	1.614
C_{23}	18.436	17.480	16.773
C_{25}	1.5813	0.527	0.615
C_{35}	-0.148	-0.707	2.661
C_{46}	0.4471	-0.607	-1.561
C_{14}	0.656	-1.168	1.875
C_{24}	2.282	1.191	-0.558
C_{56}	-1.337	-0.341	0.368

Table 8: Elastic constants (in GPa) of C-S-H (I)/AFt in z-direction.

Spacing	1 Å vacuum	3.1 Å water	6.2 Å water
C_{11}	50.815	51.560	42.498
C_{22}	45.388	44.159	44.895
C_{33}	50.441	41.135	21.202
C_{44}	4.960	6.622	2.067
C_{55}	8.521	5.364	3.994
C_{66}	10.131	8.493	10.784
C_{12}	24.680	23.541	22.966
C_{13}	21.584	19.544	11.535
C_{15}	1.785	0.852	1.151
C_{23}	23.518	19.312	14.404
C_{25}	-2.087	1.939	2.897
C_{35}	0.502	-2.000	1.978
C_{46}	-0.642	-0.173	-0.389
C_{14}	0.715	-1.602	-0.126
C_{24}	1.548	-1.730	0.608
C_{56}	0.796	-0.928	-0.745

Table 9: Elastic constants (in GPa) of C-S-H (I)/AFt counterclockwise rotated in y-direction.

Spacing	1 Å vacuum	3.1 Å water	6.2 Å water
C_{11}	51.781	47.584	42.997
C_{22}	51.781	39.976	27.623
C_{33}	45.011	39.598	43.349
C_{44}	7.143	4.283	1.862
C_{55}	11.173	8.077	10.152
C_{66}	8.140	7.410	0.145
C_{12}	20.760	18.646	12.921
C_{13}	23.981	22.570	24.148
C_{15}	0.416	-0.211	1.728
C_{23}	23.416	17.864	13.194
C_{25}	2.119	0.368	-1.489
C_{35}	0.270	-0.580	-0.016
C_{46}	-1.311	0.365	-0.097
C_{14}	0.146	1.499	1.918
C_{24}	-1.709	2.903	0.621
C_{56}	-1.313	-1.629	-0.022

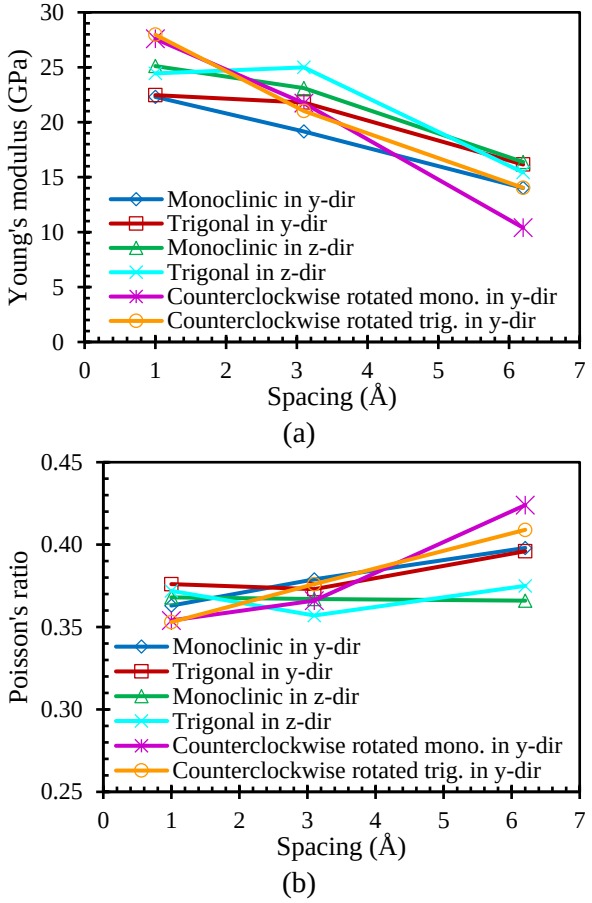

Figure 8: (a) Young's modulus, (b) Poisson's ratio in relation with spacing of C-S-H (I)/AFt composite.

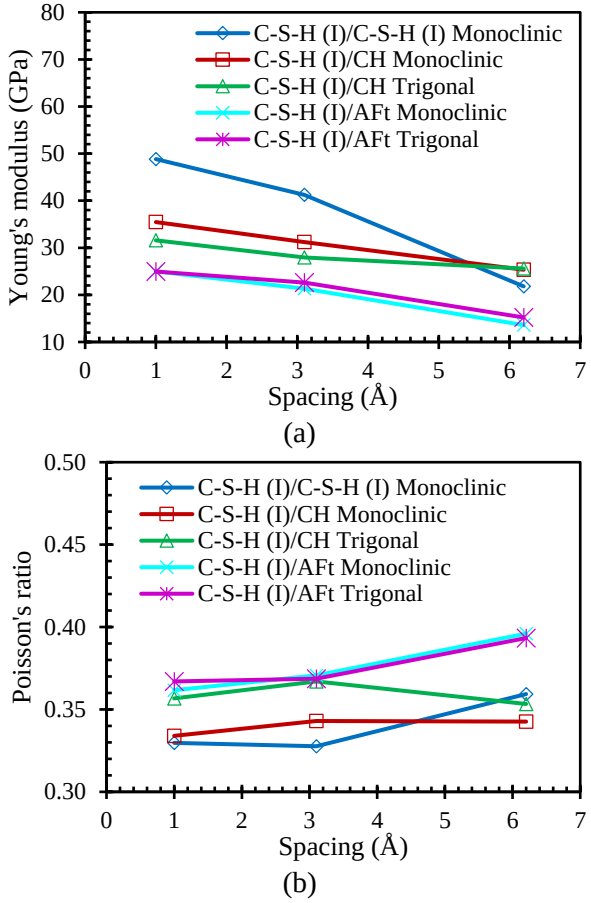

Figure 9: Average (a) Young's modulus, (b) Poisson's ratio in relation with spacing of three orientations.

With the results of Young's moduli and Poisson's ratios of different composites, it was possible to calculate Young's moduli and Poisson's ratios of simplified HCP using Mori-Tanaka scheme. The results are summarized in **Table 10**. Young's moduli and Poisson's ratios ranged from 8.1 GPa to 14.6 GPa and 0.32 to 0.36, respectively. Nevertheless, the obtained results in this study were calculated using a simplified hardened cement paste taking into account only three main hydrated cement paste phases (i.e., CH, C-S-H (I) and AFt) without considering unhydrated phases. It should be possible to use this method to calculate Young's modulus and Poisson's ratio of a normal hardened cement paste by calculating elastic constants of different composites with other hydrated and unhydrated phases.

Table 10: Young's modulus and Poisson's ratio of simplified HCP via Mori-Tanaka scheme.

Group	Spacing	E (GPa)	υ
Monoclinic	1 Å vacuum	14. 6	0.32
	3.1 Å water	12.6	0.33
	6.2 Å water	8.1	0.36
Trigonal	1 Å vacuum	14.0	0.33
	3.1 Å water	12.3	0.34
	6.2 Å water	8.4	0.36

4 CONCLUSION

In this study, elastic constants of composites made of the main hydrated cement paste phases were obtained using molecular dynamics simulation via a software called LAMMPS. From the slope of stress-strain curves with a small strain of 1%, the values of elastic constants were obtained. The deformation were applied on six different directions of composite supercells. With the values of elastic constants, Young's modulus and Poisson's ratio could be

calculated using Voigt-Reuss-Hill approximation. In order to calculate shear and bulk of Voigt and Reuss bounds, the equations are different depending upon space groups (i.e., monoclinic or trigonal). Furthermore, Young's modulus and Poisson's ratio of a simplified hardened cement paste could be calculated using Mori-Tanaka homogenization scheme. Young's moduli and Poisson's ratios are found to be in a range of 8.1 GPa to 14.6 GPa and 0.32 to 0.36, respectively. It might be possible to utilize this methodology to acquire Young's modulus and Poisson's ratio of a normal hardened cement paste by calculating elastic constants of different composites considering other unhydrated and hydrated phases.

REFERENCES

[1] D. Keinde, S. Kamali-Bernard, F. Bernard, I. Cisse, Effect of the interfacial transition zone and the nature of the matrix-aggregate interface on the overall elastic and inelastic behaviour of concrete under compression: a 3D numerical study, European Journal of Environmental and Civil Engineering. 18 (2014) 1167–1176.

[2] K. Ioannidou, Mesoscale Structure and Mechanics of C-S-H, in: W. Andreoni, S. Yip (Eds.), Handbook of Materials Modeling: Applications: Current and Emerging Materials, Springer International Publishing, Cham, 2020: pp. 1–15.

[3] D. Lau, W. Jian, Z. Yu, D. Hui, Nano-engineering of construction materials using molecular dynamics simulations: Prospects and challenges, Composites Part B: Engineering. 143 (2018) 282–291.

[4] H.F.W. Taylor, Cement chemistry, 2. ed., Repr, Telford, London, 1997.

[5] A.E. Moore, H.F.W. Taylor, Crystal structure of ettringite, Acta Cryst B. 26 (1970) 386–393.

[6] J. Fu, S. Kamali-Bernard, F. Bernard, M. Cornen, Comparison of mechanical properties of C-S-H and portlandite between nano-indentation experiments and a modeling approach using various simulation techniques, Composites Part B: Engineering. 151 (2018) 127–138.

[7] S. Kamali-Bernard, F. Bernard, Effect of tensile cracking on diffusivity of mortar: 3D numerical modelling, Computational Materials Science. 47 (2009) 178–185.

[8] A. Rhardane, F. Grondin, S.Y. Alam, Development of a micro-mechanical model for the determination of damage properties of cement pastes, Construction and Building Materials. 261 (2020) 120514.

[9] E. Del Gado, K. Ioannidou, E. Masoero, A. Baronnet, R.J.-M. Pellenq, F.-J. Ulm, S. Yip, A soft matter in construction – Statistical physics approach to formation and mechanics of C–S–H gels in cement, Eur. Phys. J. Spec. Top. 223 (2014) 2285–2295.

[10] L. Desgranges, D. Grebille, G. Calvarin, G. Chevrier, N. Floquet, J.-C. Niepce, Hydrogen thermal motion in calcium hydroxide: Ca(OH)2, Acta Cryst B. 49 (1993) 812–817.

[11] F. Goetz-Neunhoeffer, J. Neubauer, Refined ettringite (Ca6Al2(SO4)3(OH)12 ·26H2O) structure for quantitative X-ray diffraction analysis, Powder Diffraction. 21 (2006) 4–11.

[12] J. Fu, F. Bernard, S. Kamali-Bernard, Assessment of the elastic properties of amorphous calcium silicates hydrates (I) and (II) structures by molecular dynamics simulation, Molecular Simulation. 44 (2018) 285–299.

[13] S.A. Hamid, The crystal structure of the 11Å natural tobermorite Ca2.25[Si3O

7.5(OH)1.5] · 1H2O, Zeitschrift Für Kristallographie - Crystalline Materials. 154 (1981) 189–198.

[14] D. Frenkel, B. Smit, Understanding Molecular Simulation: From Algorithms to Applications, Elsevier, 2001.

[15] A.P. Thompson, H.M. Aktulga, R. Berger, D.S. Bolintineanu, W.M. Brown, P.S. Crozier, P.J. in 't Veld, A. Kohlmeyer, S.G. Moore, T.D. Nguyen, R. Shan, M.J. Stevens, J. Tranchida, C. Trott, S.J. Plimpton, LAMMPS - a flexible simulation tool for particle-based materials modeling at the atomic, meso, and continuum scales, Computer Physics Communications. 271 (2022) 108171.

[16] A.C.T. van Duin, S. Dasgupta, F. Lorant, W.A. Goddard, ReaxFF: A Reactive Force Field for Hydrocarbons, J. Phys. Chem. A. 105 (2001) 9396–9409.

[17] L. Liu, A. Jaramillo-Botero, W.A. Goddard, H. Sun, Development of a ReaxFF Reactive Force Field for Ettringite and Study of its Mechanical Failure Modes from Reactive Dynamics Simulations, J. Phys. Chem. A. 116 (2012) 3918–3925.

[18] S. Hoeun, F. Bernard, F. Grondin, S. Kamali-Bernard, S.Y. Alam, Elastic constants of nano-scale hydrated cement paste composites using reactive molecular dynamics simulations to homogenization of hardened cement paste mechanical properties, Materials Today Communications. (2023) 106671.

[19] Z. Wu, E. Zhao, H. Xiang, X. Hao, X. Liu, J. Meng, Crystal structures and elastic properties of superhard Ir N2 and Ir N3 from first principles, Phys. Rev. B. 76 (2007) 054115.

[20] J. Fu, H. Bai, Z. Zhang, W. Lin, Elastic constants and homogenized moduli of manganese carbonate structure based on molecular dynamics and Reuss-Voigt-Hill methods, IOP Conf. Ser.: Mater. Sci. Eng. 423 (2018) 012046.

[21] S. Kamali, Comportement et simulation des matériaux cimentaires en environnement agressifs: lixiviation et température, PhD Thesis, Cachan, Ecole normale supérieure, 2003.

[22] F. Bernard, J. Fu, S. Kamali-Bernard, Multiscale modelling approach to determine the specific heat of cementitious materials, European Journal of Environmental and Civil Engineering. 23 (2019) 535–551.

[23] Y. Liang, Mechanical and fracture properties of calcium silicate hydrate and calcium hydroxide composite from reactive molecular dynamics simulations, Chemical Physics Letters. 761 (2020) 138117.

[24] P.A. Bonnaud, C. Labbez, R. Miura, A. Suzuki, N. Miyamoto, N. Hatakeyama, A. Miyamoto, K.J.V. Vliet, Interaction grand potential between calcium–silicate–hydrate nanoparticles at the molecular level, Nanoscale. 8 (2016) 4160–4172.